Self-compression of optical laser pulses by filamentation

André Mysyrowicz, Arnaud Couairon, Ursulla Keller

New Journal of Physics
The open-access journal for physics

Self-compression of optical laser pulses by filamentation

A Mysyrowicz[1,4], A Couairon[2] and U Keller[3]

[1] Laboratoire d'Optique Appliquée, CNRS, École Nationale Supérieure des Techniques Avancées—École Polytechnique, F-91761 Palaiseau, France
[2] Centre de Physique Théorique, CNRS, École Polytechnique, F-91128 Palaiseau, France
[3] ETH Zurich, Physics Department / Institute of Quantum Electronics, 8093 Zurich, Switzerland
E-mail: mysyr@ensta.fr, couairon@cpht.polytechnique.fr and keller@phys.ethz.ch

New Journal of Physics **10** (2008) 025023 (14pp)
Received 24 September 2007
Published 29 February 2008
Online at http://www.njp.org/
doi:10.1088/1367-2630/10/2/025023

Abstract. During the propagation of intense femtosecond laser pulses in a transparent medium, pulse shortening can occur without external guiding. Experimental evidence for this effect and a description of its physical origin are presented. Nearly single cycle pulses at 800 nm with an energy of 0.120 mJ can be obtained with excellent beam quality. Carrier envelope offset phase (CEP) stability is conserved or even improved after the nonlinear propagation stage. Prospects for further improvement are discussed.

Contents

[4] Author to whom any correspondence should be addressed.

1. Introduction

The present laser technology based on Ti:sapphire allows routinely reproducible optical pulses in the near infrared (IR) region to be obtained with a typical duration in the range 10–100 fs. After chirped pulse amplification (CPA) [1], the energy per pulse can reach from millijoule to several joules, depending on the repetition rate. There are strong incentives to reduce the pulse duration further, on the brink of the single cycle limit (∼3 fs at 800 nm). Near single cycle optical pulses are essential ingredients in attosecond physics both for the generation of XUV attosecond pulses [2, 3] and for a short intense streaking pulse in the near IR [3, 4]. In addition, they are important in ultra-relativistic nonlinear optics, where the laser field is high enough to impart to protons a velocity close to the speed of light [5]. The ultra-relativistic nonlinear optical regime requires peak laser intensities in the range of 10^{23} W cm^{-2}. A shorter pulse could lead to drastic cost and size reduction of the laser facility, since most of the purchasing price of amplifier systems directly scales with the pulse energy.

A well developed technique for pulse compression has been used for several years. It consists in launching the pulse to be compressed into a long guiding structure (a hollow fibre) filled with a neutral gas [6]. Self phase modulation (SPM) of the pulse during guided propagation leads to a large spectral broadening. The broadened spectrum has a linear chirp since redder frequencies are added during the ascending slope of the propagating pulse while bluer frequencies are generated on the descending slope. Using an external compressor at the output yields pulses as short as 4.5 fs [7], or 3.8 fs with a dual fibre compressor [8, 9]. There are however several disadvantages with this scheme [10]. It requires meticulous alignment, is prone to hollow fibre damage and is limited in the recompressed pulse energy since plasma ionization of the gas in the hollow fibre must be avoided.

In 2004, filament compression of carrier envelope offset phase (CEP) [11] stabilized pulses in the few-cycle regime has been demonstrated in Zurich [12]. It was recognized during the tedious alignment of two successive hollow fibre compression stages that similar or even better results were obtained when the two hollow fibres were simply removed. These results were interpreted as being due to filamentation occurring during propagation in the argon inside the chambers containing the hollow chambers. Indeed, pulse reshaping of UV and IR pulses by filamentation had been reported earlier in gases and solids [13]–[16] and shown to result in shorter subpulses, but it was the first time that isolated pulses close to the single cycle limit were measured and that numerical simulations showed sub-3 fs self-compressed filaments [12, 17]. Conserved or even improved carrier-envelope phase (CEP) stability was observed after the filamentation stage [18]. In this paper, we successively review properties of filamentation and discuss why pulse compression is expected. Then experimental results concerning the production of near single cycle IR optical pulses are described and discussed. Finally, we discuss prospects for further improvements and draw some conclusions.

2. Filamentation

Consider a short pulse of central wavelength λ_0 with an input power $P > P_{cr}$ propagating in a transparent medium. Here, we consider argon, but similar effects take place in other gases, in transparent liquids or solids. P_{cr} is given by the relation $P_{cr} \equiv 3.72\lambda_0^2/8\pi n_0 n_2$ where n_0 is the index of refraction at the laser wavelength λ_0, n_2 is the nonlinear Kerr coefficient at λ_0. For argon at atmospheric pressure $n_0 = 1.0$, $n_2 = 3 \times 10^{-19}$ cm^2 W^{-1} at 800 nm so that

$P_{cr} = 3.4\,\mathrm{GW}$. The condition $P > P_{cr}$ translates the fact that beam self focusing always prevails over the defocusing effect due to diffraction. As a consequence, beam collapse is expected to occur after a propagation distance given by [19]:

$$L_c = \frac{0.367 L_{DF}}{\sqrt{[(P_{in}/P_{cr})^{1/2} - 0.852]^2 - 0.0219}},$$

where $L_{DF} = \frac{\pi n_0 w_0^2}{\lambda_0}$ is the Rayleigh length of the beam of waist w_0.

However, before beam collapse, the intensity has increased to the point that ionization of the gas occurs, in a multiphoton process involving the simultaneous absorption of 11 photons, corresponding to the energy necessary to liberate an electron from an argon atom ($11 \times 1.55\,\mathrm{eV} > U_i = 15.76\,\mathrm{eV}$). Beam collapse is therefore prevented by multiphoton absorption and the defocusing effect of the plasma. The complex interplay between diffraction, self-focusing by the optical Kerr effect, defocusing and absorption by the plasma and other effects such as pulse self-steepening leads to the formation of a filament, i.e. a pulse maintaining a narrow beam diameter ($\sim 50\,\mu\mathrm{m}$) while keeping a high intensity ($\sim 5 \times 10^{13}\,\mathrm{W\,cm^{-2}}$) over long distances $L > L_{DF}$. Filamentation is described by a set of two coupled, highly nonlinear equations for the evolution of the envelope $\varepsilon(r, t, z)$ of the laser pulse along the z-axis and that of the plasma density $\rho(r, t, z)$ generated by the intense pulse, which must be solved numerically. The derivation of the model describing the propagation of an intense pulse in ionizing transparent media and filamentation is reviewed in [20] and is similar to that performed by Brabec and Krausz [21], with specific nonlinear terms for the physical effects mentioned above:

$$2\mathrm{i}\left(k_0 + \frac{\mathrm{i}}{v_g}\frac{\partial}{\partial t}\right)\frac{\partial \varepsilon}{\partial z} + [\Delta_\perp + D]\,\varepsilon + 2\mathrm{i}k_0 N\,(\varepsilon, \rho) = 0, \tag{1}$$

$$\frac{\partial \rho}{\partial t} = W(\varepsilon)(\rho_{nt} - \rho) + \frac{\sigma}{U_i}\rho|\varepsilon|^2, \tag{2}$$

Here, $k_0 = k(\omega_0)$ denotes the wavenumber corresponding to the central frequency ω_0 and $k(\omega) = n(\omega)\omega/c$ where $n(\omega)$ is the refractive index of the medium (the Sellmeier-like dispersion relation for argon is obtained from [22]). These equations are expressed in the reference frame moving with the pulse and thus, t denotes the retarded time $\tau - z/v_g$ and $v_g \equiv \partial\omega/\partial k|_{\omega_0}$ the group velocity. The term $\Delta_\perp$ in equation (1) represents the beam diffraction; the second term D is defined from its Fourier transform in the frequency domain $\hat{D}(\omega) \equiv k^2(\omega) - \left(k_0 + v_g^{-1}(\omega - \omega_0)\right)^2$, and accounts for all dispersive terms. The last term in equation (1) represents nonlinear effects and reads as:

$$N(\varepsilon, \rho) = \mathrm{i}\frac{\omega_0}{c} n_2 T^2 |\varepsilon|^2 \varepsilon - \frac{\sigma}{2}(1 + \mathrm{i}\omega_0\tau_c)\,\rho\varepsilon - T\frac{W(\varepsilon)U_i}{2|\varepsilon|^2}(\rho_{nt} - \rho)\,\varepsilon. \tag{3}$$

The first term in equation (3) represents the optical Kerr effect. Self-steepening is accounted for through the operator $T \equiv 1 + (\mathrm{i}/\omega_0)\partial/\partial t$ in front of the Kerr term. The second term models plasma induced absorption and defocusing. The last term describes nonlinear energy losses i.e, the energy spent by the pulse for ionization. For short pulses of a few tenths of a femtosecond, optical field ionization is the dominating process for plasma generation in the filament. During filamentation, intensity usually saturates at levels which do not exceed a few $10^{14}\,\mathrm{W\,cm^{-2}}$ [23]. In this regime simulations using ionization rates $W(\varepsilon)$ described by the

Table 1. Summary of the parameters used in the simulations of equations (1) and (2).

Nonlinear index coefficient	$n_2 = 3 \times 10^{-19}\, p\ \mathrm{cm^2\ W^{-1}}$
Critical power for self-focusing	$P_{\mathrm{cr}} = 3.4 p^{-1}\ \mathrm{GW}$
Dispersion	See [22]
Ionization rate	See [20, 24, 25]
Density of argon	$\rho_{\mathrm{nt}} = 2.5 \times 10^{-19}\, p\ \mathrm{cm^{-3}}$
Critical plasma density	$\rho_{\mathrm{c}} = 1.8 \times 10^{-21}\ \mathrm{cm^{-3}}$
Collision time	$\tau_{\mathrm{c}} = 190\, p^{-1}\ \mathrm{fs}$
Cross-section for inverse bremsstrahlung	$\sigma = 7.8 \times 10^{-24}\ \mathrm{m^2}$ (at 1 atm)
Multiphoton absorption coefficient	$\beta_K = 3.4 \times 10^{-138}\, p\ \mathrm{cm^{19}\ W^{-10}}$
MPI coefficient	$\sigma_K = 5 \times 10^{-140}\ \mathrm{s^{-1}\ cm^{22}\ W^{-11}}$

Keldysh–Perelomov, Popov and Terent'ev (KPPT) formulation [24, 25] usually give satisfactory agreement with experiments (see [20] for a detailed presentation of the model). We also considered the inverse bremsstrahlung process with a cross-section of $\sigma = (e^2/n_0\varepsilon_0 m_{\mathrm{e}} c) \times \tau_{\mathrm{c}}/(1+\omega_0^2\tau_{\mathrm{c}}^2)$ according to the Drude model, where τ_{c} denotes the collision time and $\rho_{\mathrm{c}} \equiv (\varepsilon_0 m_{\mathrm{e}}/e^2)\omega_0^2$ denotes the critical plasma density.

The incoming pulse is assumed to be Gaussian in time and space and its envelope is described by:

$$\varepsilon(r, t, z=0) = \varepsilon_0 \exp\left(-\frac{r^2}{w_0^2} - \frac{t^2}{t_{\mathrm{p}}^2} - \mathrm{i}\frac{k_0 r^2}{2f}\right), \tag{4}$$

where w_0 is the beam waist, t_{p} is the pulse duration and f the effective focal length of the system.

The input intensity is computed from the input power $\varepsilon_0^2 = 2P_{\mathrm{in}}/\pi w_0^2$ and the input power P_{in} is computed from the pulse energy $P_{\mathrm{in}} = E_{\mathrm{in}}/t_{\mathrm{p}}\sqrt{\pi/2}$.

Regarding intensity saturation, multiphoton ionization (MPI) rates described by a simple power law $W(\varepsilon) = \sigma_K |\varepsilon|^{2K}$ where $K = \mathrm{mod}(U_{\mathrm{i}}/\mathrm{h}\omega_0 + 1)$ denotes the number of photons involved in the process (for argon atoms with potential $U_{\mathrm{i}} = 15.76\,\mathrm{eV}$, $K = 11$ at 800 nm) approximate well the KPPT rates and also give satisfactory agreement with experiment, even if MPI rates may be significantly larger than KPPT rates. The reason is the rapid increase of ionization rates with intensity, whereas the Kerr index increases only linearly with intensity. The estimations below will therefore rely on the MPI coefficient σ_K and its counterpart for multiphoton absorption $\beta_K = K\eta\omega_0\rho_{\mathrm{nt}}\sigma_K$, where ρ_{nt} denotes the density of neutral atoms.

Table 1 below summarizes the parameters used in our simulations and their pressure dependence [26, 27] for filamentation in an argon gas of pressure p, expressed in atm.

An important effect in self-compression by filamentation is the chirp induced by the different physical effects during propagation. Table 2 below summarizes the different contributions to calculate the chirp of a pulse, assumed to have a Gaussian profile $\varepsilon \propto \exp(-t^2/T^2)$ with flat temporal phase upon filamented propagation over a distance Δz. We consider three physical effects: group velocity dispersion (GVD) in the gas with typical length $L_{\mathrm{disp}} = T^2/2k''_0$, SPM induced by the Kerr effect and plasma induced SPM. The first line indicates for each column the phase profile in time $\phi(t)$ that would be carried by the pulse after

Table 2. Contributions to the chirp induced by different physical effects.

	GVD	Kerr-induced SPM	Plasma-induced SPM
Temporal domain $\phi(t)$	$\frac{t^2\Delta z/T^2 L_{\mathrm{disp}}}{1+\left(\Delta z/L_{\mathrm{disp}}\right)^2}$	$\frac{\omega}{c}n_2 I_{\mathrm{sat}}\exp\left(-\frac{2t^2}{T^2}\right)\Delta z$	$-\frac{\omega_0}{c}\frac{\sigma_K I_{\mathrm{sat}}^K \rho_{\mathrm{nt}}}{2n_0\rho_c}\int_{-\infty}^{t}\exp\left(-\frac{2Kt'^2}{T^2}\right)\mathrm{d}t'\Delta z$
Spectral domain $\phi(\omega)$	$\frac{k_0''(\omega-\omega_0)^2}{2}\Delta z$	$\frac{\omega}{c}\frac{\sqrt{2}}{\sqrt{3}}n_2 I_{\mathrm{sat}}\exp\left(T^2(\omega-\omega_0)^2/12\right)\Delta z$	$-\frac{\rho_{\mathrm{sat}}\omega_0^2\Delta z}{2n_0\rho_c c^2\left(k_0+v_g^{-1}(\omega-\omega_0)\right)}$
Chirp $\frac{\mathrm{d}^2\phi}{\mathrm{d}\omega^2}\vert_{\omega=\omega_0}$	$k_0''\Delta z$	$\frac{\omega_0}{c}\frac{\sqrt{2}}{\sqrt{3}}n_2 I_{\mathrm{sat}}\frac{T^2}{6}\Delta z$	$-\frac{\omega_0}{c}\frac{\rho_{\mathrm{sat}}\Delta z}{n_0^2\rho_c k_0^2 v_g^2}$
Chirp value	$2\,\mathrm{fs}^2$	$58\,\mathrm{fs}^2$	$-5\,\mathrm{fs}^2$

propagation over Δz in the absence of the other effects. The second line is the spectral phase under the same assumptions and was obtained from an approach similar to that of [26]. The third line is simply the chirp coefficient defined as the second-order derivative of the spectral phase at the central frequency. The last line gives an evaluation of the chirp coefficient for a pulse duration $T = 6\,\mathrm{fs}$ and a propagation distance of $\Delta z = 10\,\mathrm{cm}$. We used for this evaluation the saturation intensity within the filament and the plasma density given by the expressions [20, 28, 29]:

$$I_{\mathrm{sat}} = \left(\frac{2n_2\rho_c}{\sigma_K T\rho_{\mathrm{nt}}}\right)^{1/(K-1)} = 5\times 10^{13}\,\mathrm{W\,cm^{-2}}, \quad \rho_{\mathrm{sat}} = 2\rho_c n_2 I_{\mathrm{sat}} = 6\times 10^{16}\,\mathrm{cm^{-3}}.$$

These calculations are only indicative since they rely on the assumption of a decoupling between space and time. However, the calculated values for the chirp of a 6 fs pulse formed in a filament show that the Kerr-induced SPM dominates other contributions from GVD and SPM. This means that it is unlikely that a self-shortened filament carries a negative effective dispersion. Pulse compression by filamentation actually results from a reshaping process in space and time that is very similar to the transformation of a bell shaped pulse into a horseshoe pulse when it propagates in a ionizing gas [30, 31]. This mechanism will be illustrated below by the results of numerical simulations. In fact, the filamentation dynamics can hardly be described by considering space and time as independent. Several phenomena associated with filamentation are a signature of strong spatiotemporal coupling. A typical example is conical emission [32]–[36] which reflects the fact that ultrashort pulses undergoing filamentation carry angular dispersion. This angular dispersion ensures non-dispersive and non-diffractive behaviour of the self-compressed filament over some distance. This is clearly an advantage for the use of self-compressed filaments. On the other hand, little is known regarding the effect of standard optical elements (e.g. chirped mirrors) on these non-conventional pulses.

Regarding energy losses, multiphoton absorption should prevail over plasma absorption. A rough estimation can be performed from the conservation equation for the pulse energy E:

$$\frac{\partial E}{\partial z} = -\sigma\int\rho|\varepsilon|^2\mathrm{d}t\,2\pi r\,\mathrm{d}r - \beta_K\int|\varepsilon|^{2K}\mathrm{d}t\,2\pi r\,\mathrm{d}r. \tag{5}$$

By introducing a Gaussian beam and pulse shape into equation (5), one obtains

$$\frac{\Delta E}{\Delta z} = -\sigma\rho_{\mathrm{sat}} I_{\mathrm{sat}} T R^2\frac{\pi\sqrt{\pi}}{4\sqrt{2}} - \beta_K I_{\mathrm{sat}}^K T R^2\frac{\pi\sqrt{\pi}}{8K\sqrt{2K}}.$$

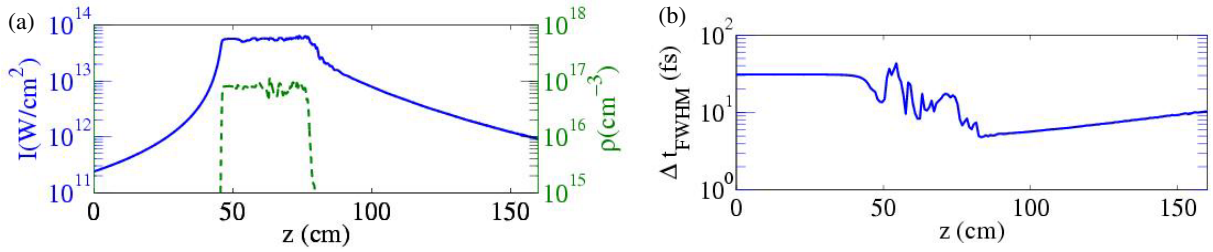

Figure 1. Typical simulation results for filamentation of a 0.9 mJ, 40 fs, 800 nm laser pulse in a 0.8 atm argon gas cell. (a) Peak intensity (solid curve, left axis) and electron density (dashed curve, right axis) as functions of the propagation distance. (b) Pulse duration defined as the full width at half maximum (FWHM) of the radially integrated temporal profile of the pulse intensity (over a radius of 100 μm).

The first term on the right-hand side corresponds to plasma absorption and the second to multiphoton absorption: for a pulse of duration $T = 6$ fs, beam width $R = 100\,\mu$m with a peak intensity of 8×10^{13} W cm^{-2}, propagating over 10 cm, the relative losses are: 240 μJ for multiphoton absorption and 2 μJ for plasma absorption.

The numerical results shown in figure 1 were obtained by solving equations (1) and (2) with parameters typical of self-compression experiments in an argon gas cell. The pulse parameters at the entrance window of the gas cell are: $w_0 = 2.7$ mm, $f = 56$ cm, $t_p = 25$ fs (FWHM 30 fs, transform limited pulse), $E_{in} = 0.9$ mJ and are standard in our experiments.

The peak intensity exhibits a 35 cm long plateau at 7×10^{13} W cm^{-2} corresponding to the filament. The density of the associated plasma channel slightly exceeds 10^{17} cm^{-3}. Figure 1(b) shows the evolution of the duration (FWHM) of the radially integrated intensity profile over a radius of 100 μm. This corresponds to the maximum value reached during propagation by the radius of the light filament, defined as the half width at half maximum of the fluence (time integrated intensity) distribution. The minimum duration of 5 fs is obtained at the end of the filament. This final duration depends on the input conditions but this self-compression behaviour is generally similar for all filaments. Under slightly different conditions, the minimum pulse duration at the end of the filament was shown to be as short as a single cycle [17]. The moving focus model [37] brings a simple explanation to this effect: self-focusing of the most powerful central part of the pulse should occur faster, hence for smaller propagation distances, than in the trailing part. In addition, self-focusing of the trailing part is delayed by plasma defocusing and therefore occurs at the end of the filament while the leading part undergoes nonlinear losses, diffraction and dispersion.

Figure 2 shows a comparison between the energy content of the filament and that of the whole pulse for the same input parameters as above. The energy calculated by integration over the whole numerical box exhibits a step-like decrease of 240 μJ (27% of the input energy) around $z = 50$ cm, which corresponds mainly to multiphoton absorption. Plasma absorption is much smaller (0.5% of the energy losses). The energy contained in the core of the 100 μm filament can be roughly evaluated to be around a few hundred microjoule (30 fs $\times 10^{14}$ W cm$^{-2} \times (100\,\mu$m$)^2 \sim 300\,\mu$J, i.e. 33% of the input energy). The dashed curve in figure 2 shows that the energy exactly computed in the filament core reaches this value at the

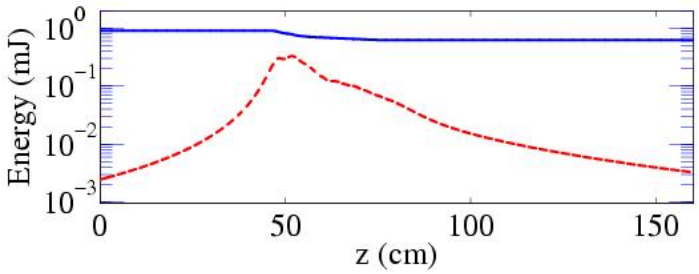

Figure 2. Evolution of the pulse energy (solid curve) and energy of the filament core (100 μm radius) during propagation (dashed curve). The pulse parameters are the same as in figure 1.

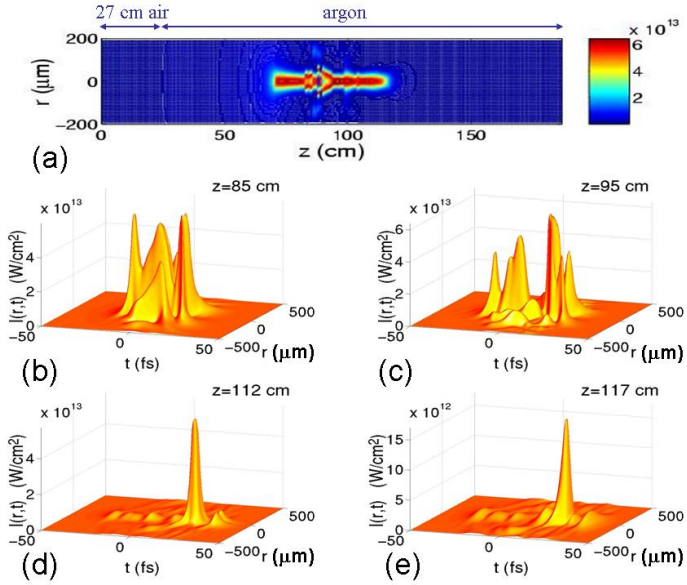

Figure 3. Dynamics of the pulse self-compression by filamentation. (a) Intensity distribution showing a 40 cm long filament. (b)–(d) Full space-time intensity profiles at four propagation distances in the filament. Here, the 800 nm, 1.1 mJ and 30 fs input pulse had a beam width $w_0 = 2.25$ mm, and was propagated in air before entering the argon gas cell at 0.8 atm (from [17]).

beginning of the filament and decreases to 50 μJ at the location of the minimum pulse duration. The energy flow is ingoing towards the core during the self-focusing stage and outgoing beyond the nonlinear focus. The part of the beam surrounding the filament core actually contains the main part of the pulse energy. Note that an optimal energy throughput is obtained at 60 cm. However, the self-compressed filament at this distance is about 10 fs, which indicates a trade-off between energy throughput and minimum pulse duration [38]. This is also in keeping with recent simulations by Kosareva *et al* [39]. As recently proposed, the pulse energy limitation could be overcome by using a planar waveguide [40].

The dynamics in the filament involves a recurrent pulse temporal splitting into shorter sub-pulses (see figure 3). Each part of the pulse which is self-focusing becomes rapidly intense and

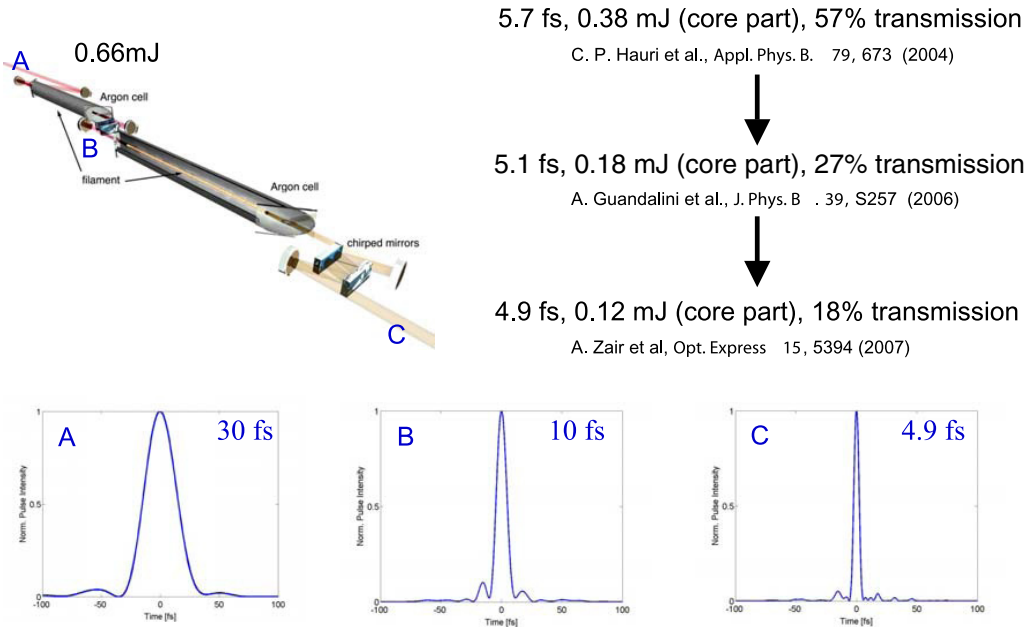

Figure 4. Experimental set-up (see text). Also shown are the pulse temporal profiles measured before the first cell (A), after the first cell and compressor (B) and after the last compressor stage (C).

eventually undergoes strong multiphoton absorption. This is the main reason for the multiple temporal splitting. Refocusing of the temporal slices of the pulse with peak power above critical occurs until the end of the filament, where this complicated dynamics gives rise to an isolated few-cycle pulse with an intensity of a few 10^{13} W cm^{-2}. This result is obtained in a broad range of input parameters.

3. Experimental results and discussion

The experimental set-up built in Zurich to produce very short pulses is shown in figure 4.

The incident CEP-locked pulses are produced in a commercial Ti:sapphire laser working at a 1 kHz repetition rate. The pulse duration is 33 fs with a maximum energy per pulse of 0.850 mJ. The beam of diameter 6.4 mm (FWHM) is focused with a −2000 radius of curvature (ROC) silver mirror inside a first 1.8 m long cell filled with Ar at a pressure of 900 mbar. After emerging from the cell, the spectrally broadened pulse is recollimated, sent through a set of chirped mirrors to remove the chirp, then focused with another −2000 ROC silver mirror into a second 1.8 m long cell filled with Ar at a pressure of 820 mbar. The emerging pulse is sent to a second set of chirped mirrors before being analysed.

Pulse duration measured with the single-shot SPIDER technique [41] is shown at the entrance, after the first cell and at the output (see figure 4). The shortest pulse which could be obtained is 4.9 fs. More careful spatio-temporal characterization revealed a trade-off between the shortest pulses and the available pulse energy: 5.7 fs (0.38 mJ, 57% transmission) [12], 5.1 fs (0.18 mJ, 27%) [18, 42] and 4.9 fs (0.12 mJ, 18%) [38]. These results are in agreement with the numerical calculations, which predict an emerging pulse with a core of duration ∼5 fs and ∼0.100 J energy, surrounded by a photon reservoir of longer duration (see figure 3).

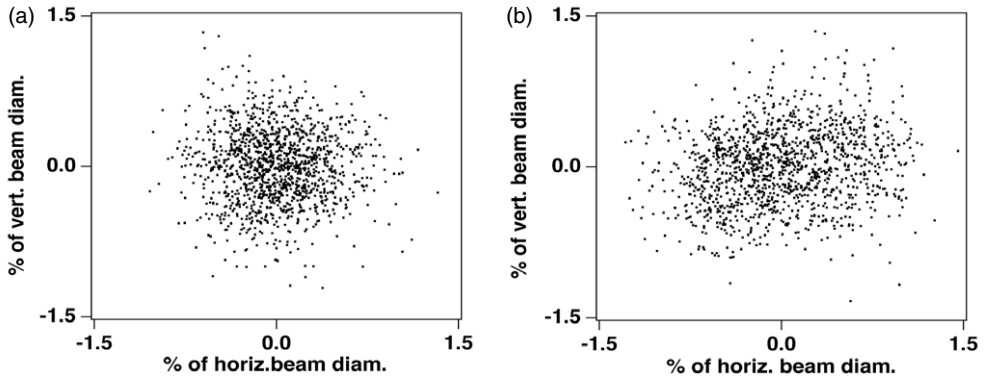

Figure 5. Beam pointing stability measured for 1500 consecutive laser pulses after a two-stage filament compressor in argon: (a) 0.5% rms without a filament (with evacuated gas cells) and (b) 0.6% rms with a filament. The two gas cells were filled with argon at 800 and 700 mbar. Similar results have been achieved at other gas pressures (according to [42]).

The compressed pulse benefits from several features of filaments: since the intensity is clamped to the ionization threshold, intensity fluctuations are reduced [43]. The beam quality is improved by a self-cleaning effect with a factor $M^2 \sim 1$ [44]. Fluctuations in the beam position have also been compared to those of a pulse propagating in vacuum. (see figure 5). No appreciable deterioration of the position stability of the filamented pulse is observed. Furthermore, a CEP-locked pulse preserves or even improves the phase stability during the two filamentary stages [18]. This result is rather surprising, in view of the complex restructuring of the pulse during filamentation. For example, such a two-state filament compressor has been successfully used for attosecond angular streaking measurements during which the intense CEP-stabilized two-cycle pulses had to be stable for several hours supporting a measurement accuracy of 23 as [4]. The CEP was stabilized at the oscillator and after the two-stage filament compressor where we could directly use the f-to-2f interferometer [11] without further spectral broadening.

4. Prospects

There is in principle still room for further pulse reduction if better chirped mirrors are used to mainly compensate for the dispersion of the Brewster-angled exit window of the Ar-cell . Initial measurements in Zurich yielded pulses of 5.7 fs duration, which could be reduced to 4.9 fs by the use of better designed chirped mirrors. The pulse spectrum measured after the second filamentation stage but before the chirped mirror compression stage can show a smooth broadband spectrum (see figure 6), with a Fourier transform pulse width of 1.75 fs (assuming a flat spectral phase). However, design and construction of broadband chirped mirrors compatible with such a bandwidth become an increasingly challenging task [45, 46]. Another approach to reach shorter pulses is described in the last paragraph.

At the present time, improvement in compressed pulse energy is limited by the onset of multifilamentation. In argon, multifilamentation occurs at $\sim$ 17 GW [47]. An approach to obtain more energetic short pulses is to organize the multifilamentary pattern [48]. For instance, by using a 0.1 J, 30 fs pulse with a top hat intensity profile, one expects $\sim$10 filament-compressed

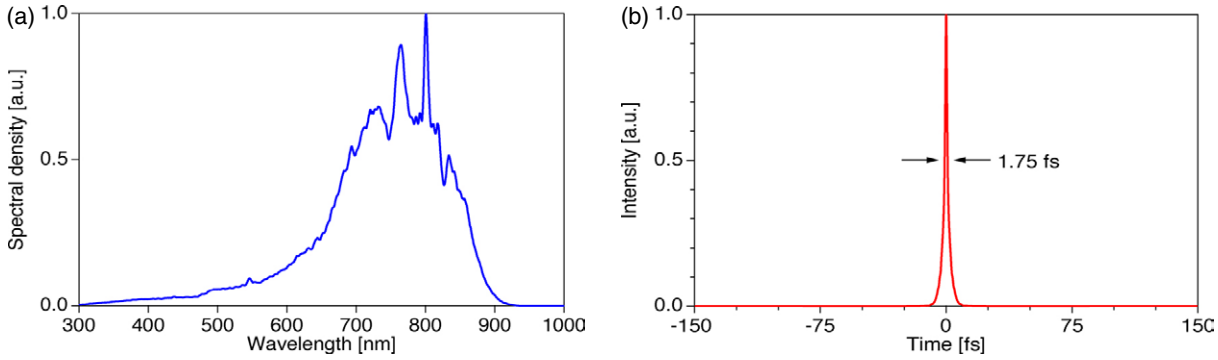

Figure 6. Two stage argon filament compressor with 0.82 mJ input pulse energy and 0.39 mJ output energy: (a) measured power spectrum of the pulse after the second compression cell but before the final compressor stage, (b) corresponding pulse duration if a constant spectral phase is assumed (according to [12]).

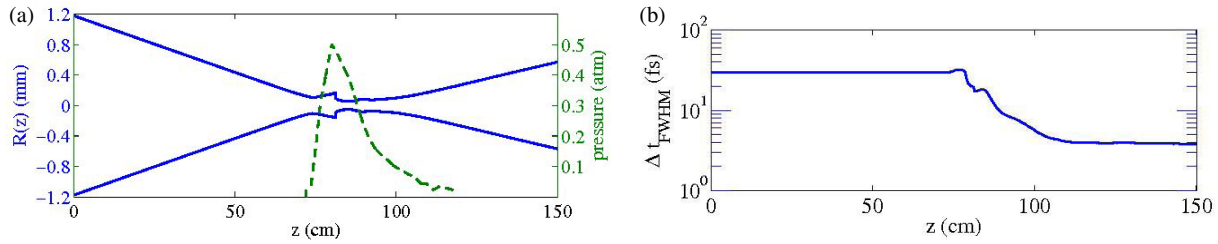

Figure 7. Self-compression in a pressure gradient. Input pulse: 1 mJ, 30 fs and 800 nm. (a) Beam width (FWHM of the fluence distribution, solid curve, left axis) and pressure gradient (dashed line, right axis) versus propagation distance. (b) Duration of the radially averaged (over 100μm) intensity profile.

pulses located on a circle. The conical emission from such organized multiple filaments shows interference effects, indicating that it should be possible to add them coherently [49]. Therefore, increase of peak intensity by two orders of magnitude could be obtained by focusing these synchronous multiple compressed pulses on target.

Another improvement concerns the extraction of the compressed pulse and its delivery on target. The transport of very short self-compressed pulses is delicate in the present scheme since transmittance through an exit window introduces dispersion which needs to be compensated, e.g. by means of recompression mirrors beyond the gas cell. To optimize the transport of the self-compressed filament, we proposed to propagate the laser pulse in a gas density gradient which allows control of the nonlinear properties of the medium via the gas pressure [50]. The gradient is shaped so as to form the filament and stop it immediately after the plasma induced self-compression. The process ends up with a short pulse delivered directly in vacuum. Figure 7(a) shows an example of pressure gradient (dashed green line) with three control parameters, the maximum pressure of the gas, the length of the gradient and the position of the pressure gradient with respect to the focus (at 80 cm) of the lens. These parameters were optimized by numerical experiments so as to reach the shortest self-compressed filament with the best contrast. The gradient shown in figure 7(a) was actually measured in a pressure gradient

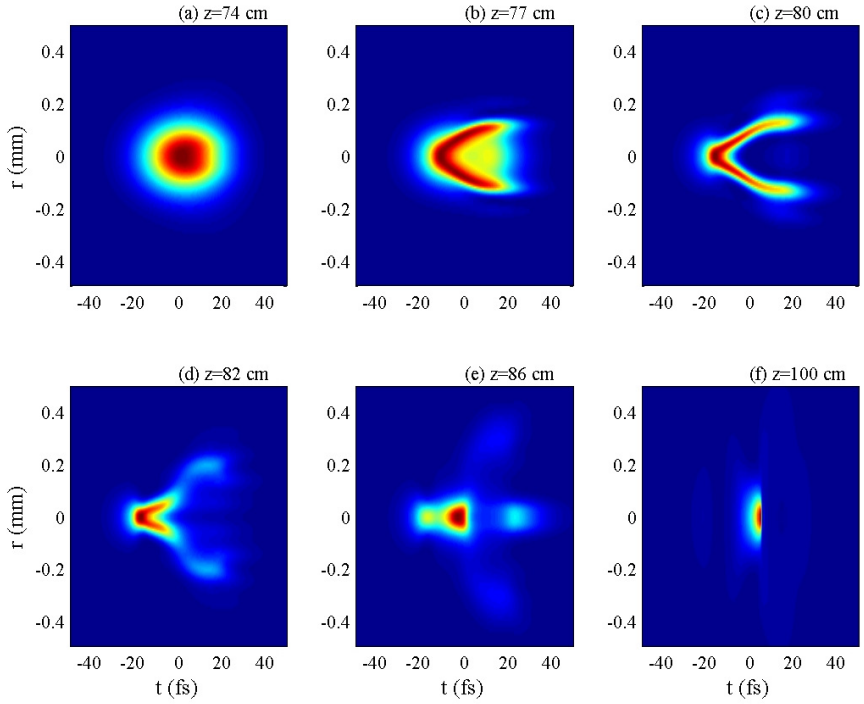

Figure 8. Pulse dynamics in space and time during self-compression in the pressure gradient for the same parameters as in figure 7.

cell specifically designed to reproduce the optimal profile [50]. Simulations performed with this measured pressure gradient predict the following results: the beam width plotted as a solid curve exhibits a small-scale filament around the maximum pressure. The pulse duration was computed by integration of the intensity over a 100 μm diameter, which contains the filament. Figure 7(b) shows the decrease of the pulse duration down to 4 fs along the propagation distance. A nearly single cycle pulse is finally obtained in vacuum. Note that no external compressor stage is required in this scheme and that the self-compression by filamentation predicted to occur in the real pressure gradient is nearly as efficient as that predicted in the ideal bi-Gaussian pressure gradient [50].

The complete dynamics in space and time of this single cycle pulse generation is shown in figure 8. Initially, the beam is focused and self-focused. Once the nonlinear focus is reached (figure 8(a)), a plasma is generated on the trail of the pulse which defocuses the light on-axis, thus generating a V-shaped pulse, i.e a cone in space-time by keeping in mind the revolution symmetry (figures 8(b) and (c)). At this stage, a cell at constant pressure would lead to a refocusing of the trail on-axis; here, the decrease of the pressure leads to the progressive extinction of the Kerr effect, thus preventing refocusing, and all higher order nonlinear effects (plasma generation and nonlinear losses) are switched off even faster (figures 8(d) and (e)). The pulse finally takes the shape of a pancake while the pressure decreases since the still intense part of the wave moves slower than the wings. This nearly single-cycle pancake keeps its duration and only diffracts in vacuum (figure 8(f)). Thus, pressure gradients constitute a very efficient mechanism to control the filamentation process and to stop it immediately after the generation of a single cycle pulse.

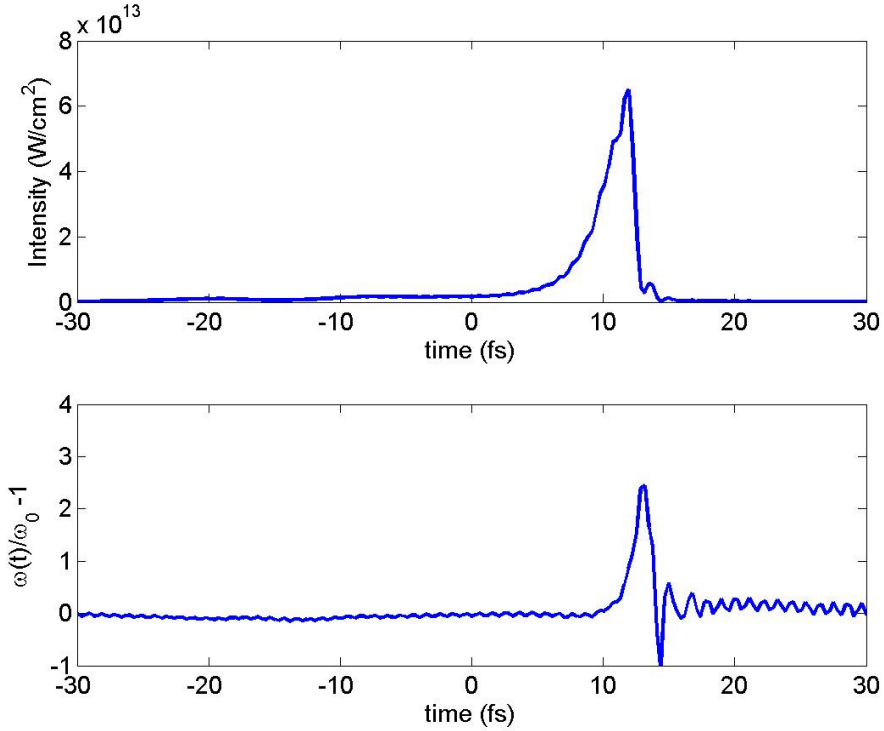

Figure 9. Typical intensity profile (top) and instantaneous frequency (bottom) for a self-compressed filament. This example was obtained from the self-compressed filament extracted from an argon gas cell with an optimized bi-Gaussian pressure gradient [50]. The pulse parameters are the same as in figure 7.

Finally, the self-compression scheme suggests that filamentation can serve a dual purpose, to shorten incident pulses and in the same cell to generate high harmonics, allowing attosecond pulse generation. High-order harmonics were shown to be generated in Xe with filamented pulses by Lange *et al* [23]. With self-compressed filaments down to a few cycles, the time dependent frequency constitutes another remarkable feature worth presenting for its consequences on attosecond pulse generation: it is well known that a laser pulse propagating in an ionizing gas undergoes frequency blueshift. In a filament, the plasma is significant only in the trail of the pulse. For a self-compressed filament, figure 9 shows that the instantaneous frequency exceeds $3\omega_0$ at the peak of the pulse and abruptly decreases in the trail. This means that self-compressed filaments can be viewed as gates in both time and frequency. With a self-compressed filament in a uniform pressure gas cell of Ne serving as driving pulse for high harmonics generation (HHG) in argon Chakraborty *et al* [51] predicted from numerical simulations that isolated 560 as XUV pulses should be obtained by spectral selection of a $10\omega_0$ range of harmonics beyond the cutoff. The rising edge of this isolated XUV emission is shaped by the increase of the intensity of the driving self-compressed filament. XUV emission stops before the peak of the driving pulse when the frequency becomes so large that it significantly reduces the cutoff energy in the spectrum of the generated harmonics with respect to that obtained for a non-chirped pulse with the same intensity. The pressure gradient

scheme described above would be especially useful for a dual operation of pulse-compression by filamentation and HHG. It would also make it easy to overcome the femtosecond barrier.

We conclude by mentioning that pulse self-compression by filamentation is still in its early stage of development but it already shows promising potential. Progress can be expected in the coming years.

Acknowledgments

We thank many collaborators, postdoctorals and graduate students who are recognized by their papers referenced throughout this invited review paper. This work was supported by NCCR Quantum Photonics (NCCR QP), research instrument of the Swiss National Science Foundation (SNSF) and the French National Centre of Scientific Research (CNRS).

References

[1] Strickland D and Mourou G 1985 *Opt. Commun.* **56** 219
[2] Hentschel M, Kienberger R, Spielmann Ch, Reider G A, Milosevic N, Brabec T, Corkum P, Heinzmann U, Drescher M and Krausz F 2001 *Nature* **414** 509
[3] Kienberger R *et al* 2004 *Nature* **427** 817
[4] Eckle P, Smolarski M, Schlup P, Biegert J, Staudte A, Schöffler M, Muller H G, Dörner R and Keller U 2007 Attosecond angular streaking *Nature* submitted
[5] Mourou G A, Tajima T and Bulanov S V 2006 *Rev. Mod. Phys.* **78** 309
[6] Nisoli M, de Silvestri S, Svelto O, Szipocs R, Ferencz K, Sielmann Ch, Sartania S and Krausz F 1997 *Opt. Lett.* **22** 522
[7] Nisoli M *et al* 1997 *Appl. Phys.* **65** 189–196
[8] Schenkel B, Biegert J, Keller U, Vozzi C, Nisoli M, Sansone G, Stagira S, De Silvestri S and Svelto O 2003 *Opt. Lett.* **28** 1987
[9] Cavalieri A L *et al* 2007 *New J. Phys.* **9** 242
[10] Gallmann L, Pfeifer T, Nagel P M, Abel M J, Neumark D M and Leone S R 2007 *Appl. Phys.* B **86** 2503
[11] Telle H R, Steinmeyer G, Dunlop A E, Stenger J, Sutter D H and Keller U 1999 *Appl. Phys.* B **69** 327
[12] Hauri C P, Kornelis W, Helbing F W, Heinrich A, Couairon A, Mysyrowicz A, Biegert J and Keller U 2004 Generation of intense, carrier-envelope phase-locked few-cycle laser pulses through filamentation *Appl. Phys.* B **79** 673
[13] Lange H R, Ripoche J-F, Chiron A A, Lamouroux B, Franco M A, Prade B, Nibbering E T J and Mysyrowicz A 1998 Time space self-compression of femtosecond laser pulses in air *CLEO/IQEC (3–8 May)*
[14] Tzortzakis S, Lamouroux B, Chiron A, Moustaizis S D, Anglos D, Franco M, Prade B and Mysyrowicz A 2001 Femtosecond and picosecond ultraviolet laser filaments in air: experiments and simulations *Opt. Commun.* **197** 131
[15] Tzortzakis S, Sudrie L, Franco M, Prade B, Mysyrowicz A, Couairon A and Bergé L 2001 *Phys. Rev. Lett.* **87** 213902
[16] Couairon A, Méchain G, Tzortzakis S, Franco M, Lamouroux B, Prade B and Mysyrowicz A 2003 *Opt. Commun.* **225** 177
[17] Couairon A *et al* 2006 Self-compression of ultra-short laser pulses down to one optical cycle by filamentation *J. Mod. Opt.* **53** 75
[18] Guandalini A *et al* 2006 5.1 fs pulses generated by filamentation and carrier envelope phase stability analysis *J. Phys. B: At. Mol. Opt. Phys.* **39** 257
[19] Marburger J H 1975 *Prog. Quantum Electron.* **4** 35

[20] Couairon A and Mysyrowicz A 2007 *Phys. Rep.* **441** 47
[21] Brabec T and Krausz F 1997 *Phys. Rev. Lett.* **78** 3282
[22] Dalgarno and Kingston 1966 *Proc. R. Soc. Lond.* A **259** 424
[23] Lange H R, Chiron A, Ripoche J-F, Mysyrowicz A, Breger P and Agostini P 1998 *Phys. Rev. Lett.* **81** 1611
[24] Keldysh L V 1965 *Sov. Phys.—JETP* **20** 1307
[25] Perelomov A M, Popov V S and Terent'ev M V 1966 *Sov. Phys.—JETP* **23** 924
[26] Liu J, Schroeder H, Chin S L, Li R, Yu W and Xu Z 2005 *Phys. Rev.* A **72** 053817
[27] Méchain G, Olivier T, Franco M, Couairon A, Prade B and Mysyrowicz A 2006 *Opt. Commun.* **261** 322
[28] Couairon A, Franco M, Méchain G, Olivier T, Prade B and Mysyrowicz A 2006 *Opt. Commun.* **259** 265
[29] Couairon A 2003 *Phys. Rev.* A **68** 015801
[30] Sergeev A, Vanin E, Stenflo L, Anderson D, Lisak M and Quiroga-Teixeiro M L 1992 *Phys. Rev.* A **46** 7830
[31] Chessa P, De Wispelaere E, Dorchies F, Malka V, Marquès J R, Hamoniaux G, Mora P and Amiranoff F 1999 *Phys. Rev. Lett.* **82** 552
[32] Nibbering E T J *et al* 1996 *Opt. Lett.* **21** 62
[33] Faccio D, Porras M A, Dubietis A, Tamosauskas G, Kucinskas E, Couairon A and Di Trapani P 2006 *Opt. Commun.* **265** 672
[34] Couairon A, Gaizauskas E, Faccio D, Dubietis A and Di Trapani P 2006 *Phys. Rev.* E **73** 016608
[35] Faccio D, Porras M A, Dubietis A, Piskarkas A, Couairon A and Di Trapani P 2006 *Phys. Rev. Lett.* **96** 193901
[36] Bragheri F, Faccio D, Couairon A, Matijosius A, Tamosauskas G, Varanavicius A, Degiorgio V, Piskarskas A and Di Trapani P 2007 *Phys. Rev.* A **76** 025801
[37] Brodeur A *et al* 1997 *Opt. Lett.* **22** 304
[38] Zaïr A *et al* 2007 Spatio-temporal characterization of few-cycle pulses obtained by filamentation *Opt. Express* **15** 5394
[39] Kosareva O G, Murtazin I N, Panov N A, Savel'ev A B, Kandidov V P and Chin S L 2007 *Laser Phys.* **4** 126
[40] Nurhuda M *et al* 2007 *Phys. Rev. Lett.* **97** 153902
[41] Kornelis W, Biegert J, Tisch J W G, Nisoli M, Sansone G, Vozzi C, De Silvestri S and Keller U 2003 *Opt. Lett.* **28** 281
[42] Hauri C P *et al* 2005 Generation of intense few-cycle laser pulses through filamentation—parameter dependence *Opt. Express* **13** 7541
[43] Becker A, Aközbek N, Vijayalakshmi K, Oral E, Bowden C M and Chin S L 2001 Intensity clamping and re-focusing of intense femtosecond laser pulses in nitrogen molecular gas *Appl. Phys.* B **73** 287
[44] Prade B *et al* 2006 Spatial mode cleaning by femtosecond filamentation *Opt. Lett.* **31** 2601
[45] Kärtner F X *et al* 1997 *Opt. Lett.* **22** 831
[46] Matuschek F X *et al* 2000 *Appl. Phys.* B **71** 509
[47] Akturk S, D'Amico C, Franco M, Couairon A and Mysyrowicz A 2007 *Opt. Express* **15** 15260
[48] Méchain G, Couairon A, Franco M, Prade B and Mysyrowicz A 2004 *Phys. Rev. Lett.* **93** 35003
[49] Cook K, Kar A K and Lamb R A 2003 *Appl. Phys. Lett.* **83** 3861
[50] Couairon A *et al* 2005 Pulse self-compression to the single-cycle limit by filamentation in a gas with a pressure gradient *Opt. Lett.* **30** 2657
[51] Chakraborty H S, Gaarde M B and Couairon A 2006 Single attosecond pulses from high harmonics driven by self-compressed filaments *Opt. Lett.* **31** 3662